Request for a CLAS approved analysis note for the exclusive electroproduction of the f_0 and f_2 mesons on the proton from the e1-6 data.

B. Guegan, M. Guidal, H.-S. Jo, A. Marti, C. Munoz,
S. Niccolai, D. Sokhan
IPN Orsay

1 Introduction

This note is written to request a CLAS Approved Analysis (CAA) from the CLAS collaboration. We want to analyze the exclusive $ep \to ep\pi^+\pi^-$ reaction from the e1-6 data set, focusing on the particular processes $ep \to epf_0(980)$ and $ep \to epf_2(1270)$. The Particle Data Group [1] states that the $\pi\pi$ channel is the "dominant" decay mode of the (scalar-isoscalar) $f_0(980)$ (the other cited decay modes such as $K\bar{K}$ or $\gamma\gamma$ being only "seen") with a width of about 50 MeV ("width determination very model dependent" [1]). The (tensor-isoscalar) $f_2(1270)$ meson is somewhat better known with a quoted fitted width of $185.1^{2.9}_{2.4}$ MeV and a $\pi\pi$ branching ratio of $84.8^{2.4}_{1.2}$ % [1].

We draw attention on the fact that these two exclusive processes $ep \to epf_0(980)$ and $ep \to epf_2(1270)$ have never been measured so far. These channels are interesting for several reasons. The $f_0(980)$ is a rather "enigmatic" state. There are several hypothesis about its nature: is it a "standard" $q\bar{q}$ meson, a 4-quark state, a glueball, a $K\bar{K}$ molecule, any combination of those,... ? [2]. Studying the Q^2-dependence of the $ep \to epf_0(980)$ can possibly provide new insights on this puzzle. For instance, in Ref. [3], a model for f_0 photoproduction in terms of Reggeized t-channel meson exchange has been developed (see Fig. 1 left) and leads to different shapes and magnitudes of the differential cross section $\frac{d\sigma}{dt}$ depending on the nature of the f_0 meson. Extending such calculation to electroproduction with, for instance, the introduction of (transition) electromagnetic form factors, which can be anticipated to have different Q^2-dependence

depending on the nature of the f_0 meson, should certainly bring additional constraints. To the knowledge of the authors, such theoretical model/calculation for f_0 *electroproduction* does not exist presently.

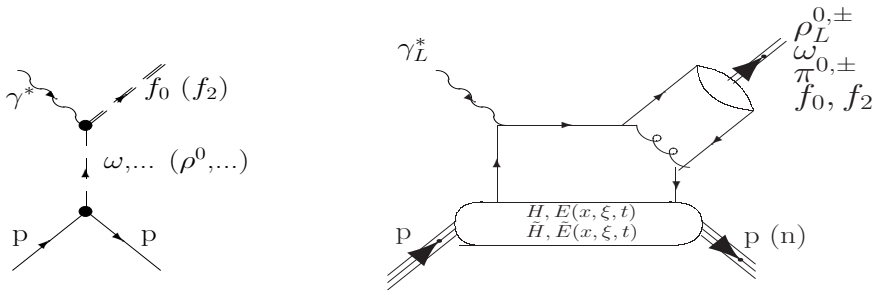

Figure 1: Mechanisms for the exclusive electroproduction of the f_0 and f_2 mesons. Left: based on "hadronic" degrees of freedom, through $t-$channel mesons Regge trajectory exchanges. Right: based on "partonic" degrees of freedom, through the "handbag" diagram and GPDs.

The nature of the $f_2(1270)$ meson is less controversial but still, there are conjectures that it could not be a "standard" $q\bar{q}$ state and rather be a dynamically generated state from vector meson-vector meson interactions [4]. Measuring the Q^2-dependence of the $ep \to epf_2(1270)$ could also certainly help to clarify the situation.

It is also interesting to analyze the two processes $ep \to epf_0(980)$ and $ep \to epf_2(1270)$, at large Q^2, in terms of Generalized Parton Distributions (GPDs) and of the handbag diagram formalism [5] (see Fig. 1 right). We recall that a broad experimental program on Deep Virtual Meson Production (DVMP), aimed at studying GPDs, is under way at JLab. Some channels have already led to publication: exclusive π^+ [6], exclusive π^0 [7] (Hall A), exclusive ρ^0 [8], exclusive ω [9], exclusive ϕ [10] (all on proton targets). Some other channels are in the final stages of the analysis: exclusive ρ^+ [11], exclusive π^0 [12] (Hall B),...

As it is well known, at leading twist, the vector meson channels are sensitive to the "unpolarized" GPDs (H and E) while the pseudo-scalar meson channels are sensitive to the "polarized" GPDs ($\tilde{H}$ and $\tilde{E}$). For scalar mesons such as f_0, the only difference with the neutral pseudo-scalar meson case is the absence of a γ^5 matrix in the Distribution Amplitude (DA) and the factorization is also twist-2 level. Because of the change of parity, the scalar channel is sensitive to the "unpolarized" GPDs, H and E, providing, complementary to vector mesons, access to these latter GPDs.

For tensor mesons such as f_2, the situation depends on the helicity of the final state f_2:

- For helicity 0 f_2's, the case is identical to the case of *longitudinal* ρ^0 electroproduction. There is factorisation at the twist-2 level and the reaction is sensitive to the "unpolarized" GPDs H and E.
- For helicity ± 1 f_2's, one has a twist-3 DA (like *transverse* ρ^0 electroproduction) and the factorisation is therefore not demonstrated. Possibly, a (model-dependent) higher-twist interpretation "a la Kroll-Goloskokov" [13] can be attempted.
- For helicity ± 2 f_2's, one has a twist-2 DA having two components: a "standard" $q\bar{q}$ component as well as a 2-gluon [14] (see Fig. 2 left). This means that there is an additional "handbag" diagram, besides the one of Fig. 1 right, contributing to the $ep \to epf_2(1270)$ process. This additional mechanism is shown in Fig. 2 right. It is shown in Ref. [15, 16] that this latter mechanism should be dominant over the mechanism of Fig. 1 right. Therefore, one can get information about the gluonic component of the f_2 meson in studying the process $ep \to epf_2(1270)$ at large Q^2 in the valence region, where quark exchange mechanisms of the type of Fig. 1-right and Fig. 1-right dominate.

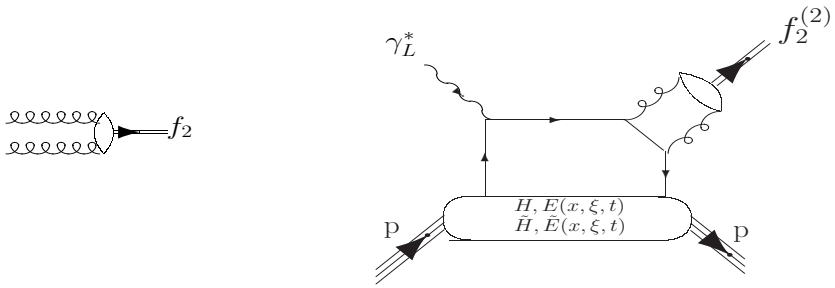

Figure 2: Left: gluon contribution to the f_2 DA. Right: dominating leading order diagram for the exclusive electroproduction of a *helicity-2* f_2 on the proton.

More generally, the whole process $ep \to ep\pi^+\pi^-$, i.e. beyond the two particular resonant states $f_0(980)$ and $f_2(1270)$, can lend itself to a handbag diagram and GPD interpretation. The meson DA should then be replaced by a "2π DA", also called a "Generalized Distribution Amplitudes" (GDA) [17, 18]. GDAs are QCD non-perturbative structure functions which describe the fragmentation of a pair of collinear partons (quarks or gluons) into a pair of pions.

In this document, we focus on the two particular exclusive $ep \to epf_0(980)$ and $ep \to epf_2(1270)$ channels. In the following, we present the results of a rapid and sketchy data analysis of the CLAS e1-6 data in order to show that

this analysis is definitely feasible. A refined and definitive data analysis requires more work and this is why we request a CAA.

2 Rapid analysis of the e1-6 data

The e1-6 data were taken from October 2001 to January 2002 with an electron beam energy of 5.754 GeV impinging on an unpolarized 5-cm long liquid-hydrogen target in the CLAS detector. The integrated luminosity of this data set was about 28.5 fb^{-1}. The kinematic domain of the selected sample corresponds approximatively to Q^2 from 1.5 GeV^2 to 5.5 GeV^2 and $W < 3$ GeV.

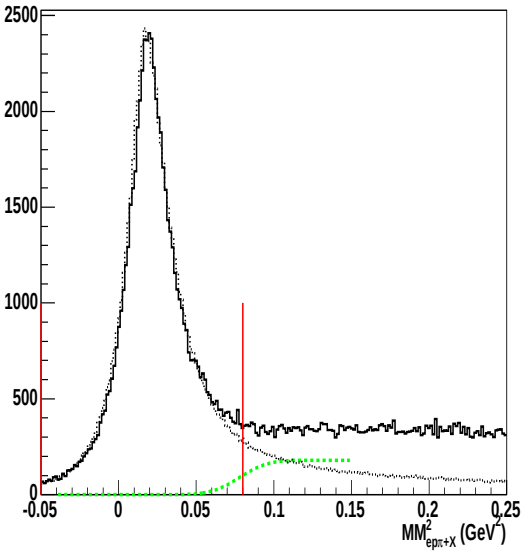

Figure 3: $M_X^2[e^-p\pi^+X]$ for $W \geq 1.8$ GeV and $E' \geq 0.8$ GeV. The red lines indicate the cut applied to select the $e^-p \to e^-p\pi^+\pi^-$ final state. The dotted line shows the simulated spectra of the two-pion channel $e'p\pi^+\pi^-$ and the green dashed line shows the simulated spectra of the three-pion channel $e'p\pi^+\pi^-\pi^0$, normalized to the data.

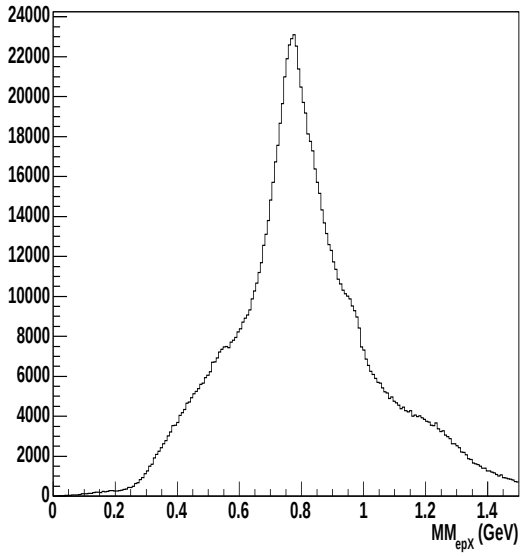

Figure 4: Missing mass $M_X[e'pX]$ for -0.05 $\leq$ $M_X^2[e'p\pi^+]$ $\leq$ 0.08 GeV^2, $W \geq 1.8$ GeV and $E' \geq 0.8$ GeV. The $\rho^0(770)$ as well as the $f_0(980)$ and $f_2(1270)$ resonances which can be distinguished sit on top of a background of non-resonant two-pion continuum.

Our group originally analyzed this data set in order to study the $ep \to ep\rho^0 \hookrightarrow \pi^+\pi^-$ reaction. We extracted various kinematical dependences (W, x_B, Q^2, t,...) of the total and differential cross-sections. The results were published in Ref. [8]. In this analysis, we detected the scattered electron, the

recoil proton and the π^+. After proper identification of these three particles, the exclusive final state $ep \to p\pi^+\pi^-$ was selected by requiring a missing π^-. Fig. 3 shows the squared missing mass $M_X^2(ep\pi^+)$ where the peak of the missing π^- is clearly visible, with very little contamination from the 3-pion final state processes. The invariant mass of the $\pi^+\pi^-$ (or equivalently the missing mass of the epX system) could then be formed and is displayed in Fig. 4 for all of our data. In this figure, on the one hand, one can clearly see the broad dominant ρ^0 resonance and, on the other hand, one can distinguish hints of "bumps" for the $f_0(980)$ and $f_2(1270)$ mesons.

If we separate the data in different (x_B, Q^2) bins, the $f_0(980)$ and $f_2(1270)$ peaks/bumps become much more visible, as can be seen in Fig. 5. In this figure, originally from our ρ^0 analysis and slightly revisited/reanalyzed here [1], the data are normalized and corrected for CLAS acceptance and efficiency so that one can directly extract cross sections in μbarn. These $\pi^+\pi^-$ invariant mass spectra were fitted independently in each (x_B, Q^2) bin by a sum of four functions: three (skewed) Breit-Wigners to describe the evident three mesonic π^+-π^- resonant structures of the $\rho^0(770)$, $f_0(980)$ and $f_2(1270)$ and one (smoothed) histogram representing the $M_{\pi^+\pi^-}$ projection of the phase-space process $e^-p \to e^-p\pi^-\pi^+$ aimed at representing the non-resonant π^+-π^- continuum. This procedure is clearly model dependent. For instance, it doesn't take into account interference effects between the meson resonances and the large background underneath since all the different channels are summed at the cross-section level. Also, the representation of the non-resonant π^+-π^- continuum by a phase space spectrum is too simplistic since many channels, such as πN^* or $\pi\Delta^*$ electroproduction (for instance $e^-p \to e^-\Delta^{++}\pi^- \hookrightarrow p\pi^+$), contribute to the $e^-p \to e^-p\pi^-\pi^+$ reaction and might produce π^+-π^- invariant mass spectra with a different shape than simple phase space. In Ref. [8], we estimated and assigned a $\approx 20\%$ systematic uncertainty due to this model-dependency issue which turned out to be the dominant contribution to the error bars of our extracted cross sections. This being said, the integral of each Breit-Wigner in Fig. 5 gives then access to the cross section of the $ep \to ep\rho^0$, $ep \to epf_0(980)$ and $ep \to epf_2(1270)$ reactions for each (x_B, Q^2) bin.

With the following definitions:

$$\sigma_{\gamma^* p \to p(\rho^0, f_0, f_2)}(Q^2, x_B, E) = \frac{1}{\Gamma_V(Q^2, x_B, E)} \frac{d^2\sigma_{e^-p \to e^-p(\rho^0, f_0, f_2)}}{dQ^2 dx_B} \tag{1}$$

$$\Gamma_V(Q^2, x_B, E) = \frac{\alpha}{8\pi} \frac{Q^2}{m_p^2 E^2} \frac{1 - x_B}{x_B^3} \frac{1}{1 - \epsilon} \tag{2}$$

and

$$\epsilon = \frac{1}{1 + 2\frac{Q^2 + (E - E')^2}{4EE' - Q^2}} \tag{3}$$

[1] The only changes made here are the fits in Fig. 5. The ranges in which the centroids and the widths of the three Breit-Wigners (ρ^0, f_0 and f_2) are allowed to vary have been varied in order to test how robust were the f_0 and f_2 fits.

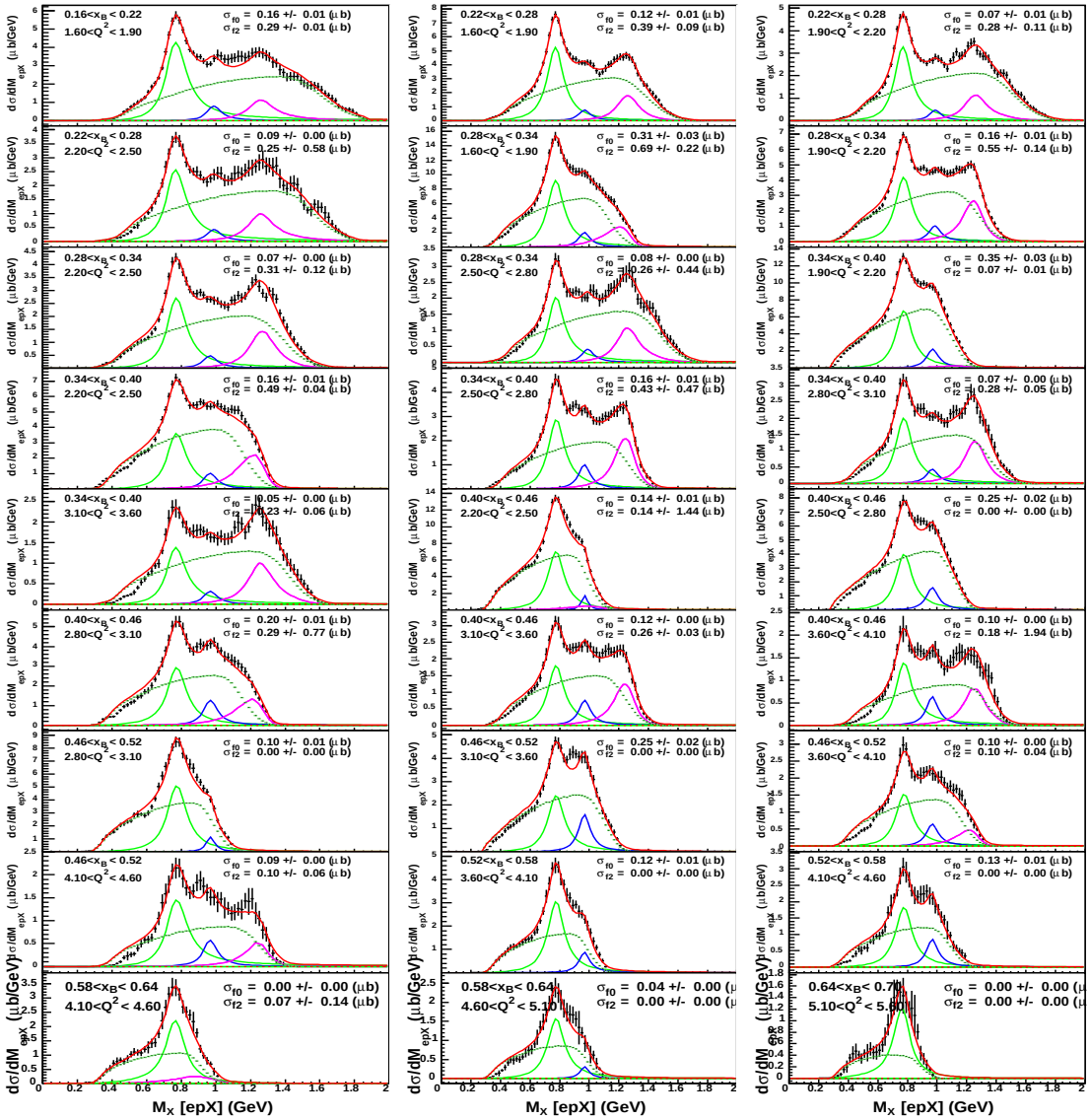

Figure 5: $M_X[e^-pX]$ acceptance-corrected and normalized distributions, showing fits for the background subtraction. In red : total fit result; in green : ρ^0 contribution; in blue : f_0 contribution; in purple : f_2 contribution and in dotted green: the projection on $M_{\pi^+\pi^-}$ of the phase space $e^-p \to e^-p\pi^-\pi^+$ contribution.

one can extract the "reduced" cross sections $\sigma_{\gamma^* p \to p(\rho^0, f_0, f_2)}$. We present them as a function of Q^2 at fixed x_B in Fig. 6 (the ρ^0 cross sections were already published in Ref. [8]).

All cross sections decrease with Q^2 as could be expected and we see that the ρ^0 cross section is the dominant one, followed by the f_2 and the f_0. In Fig. 7, we show these same cross sections as a function of W at fixed Q^2. All cross sections

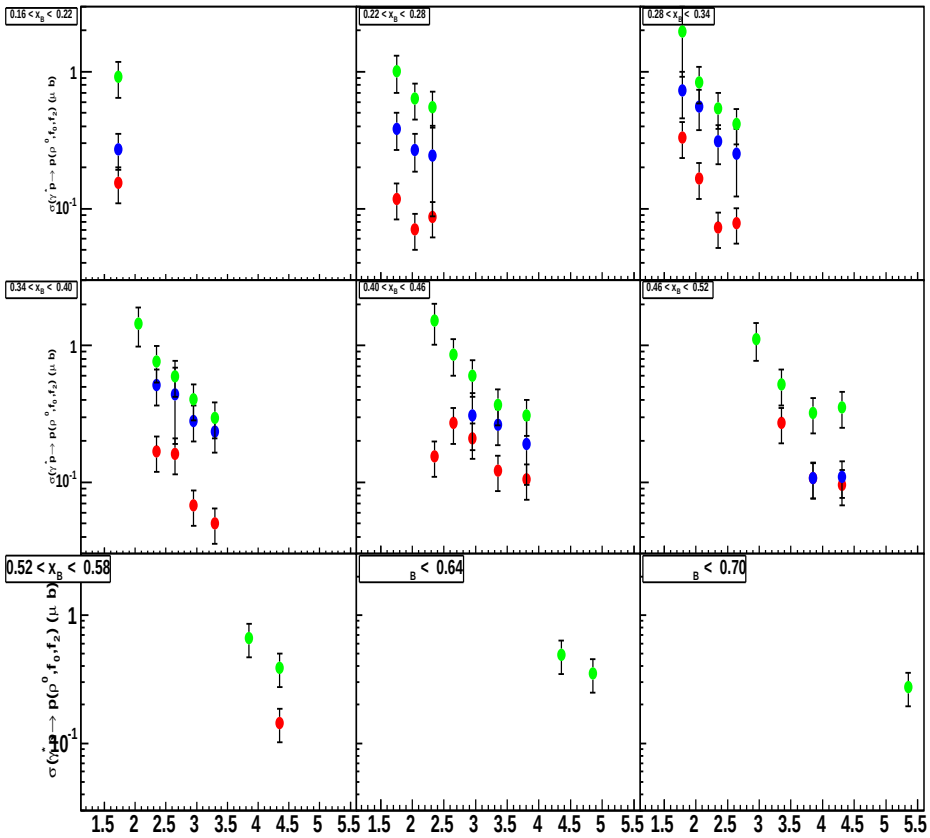

Figure 6: Reduced cross sections $\gamma^* p \to p\rho^0$ (green), $\gamma^* p \to p f_0$ (blue) and $\gamma^* p \to p f_2$ (red) as a function of Q^2 for constant W bins, in units of μbarn. The error bars include the quadrature addition of statistical and of the systematic uncertainties discussed in the text.

decrease with W, hinting at a reaction mechanism based on some meson or $q\bar{q}$ exchange in the t-channel for all three channels.

We also started to analyze the decay angular distribution of the f_0 and f_2 mesons in their center of mass frame (with the z-axis oriented along the f_0 or f_2 direction in the $\gamma^* - p$ center-of-mass system, i.e. the so-called "Helicity Frame" -HS-, see Fig. 8). By fitting with the same procedure described above the $\pi^+\pi^-$ invariant mass spectra for each (x_B,Q^2, $\cos(\theta_{HS})$) bins (where θ_{HS} is the polar angle in the HS frame), we extracted the angular distributions presented in Fig. 9 (for the f_0) and Fig. 10 (for the f_2). In Fig. 9, it is seen that for all (x_B,Q^2) bins, the $\cos(\theta_{HS})$ distribution is flat, confirming that the decay pions originate from a spin-0 particle. This provides an important model-independent cross-check of our analysis, giving us trust that our "simplistic" extraction of the f_0 signal from the $\pi^+\pi^-$ background/continuum is correct at the first order.

In Fig. 10, the decay-pion angular distribution is shown for each (x_B,Q^2) bin for the f_2. One sees that the shapes are not flat and show some structures. This could be expected since the f_2 is a spin-2 meson. Explicitely, if the f_2 is produced in a :

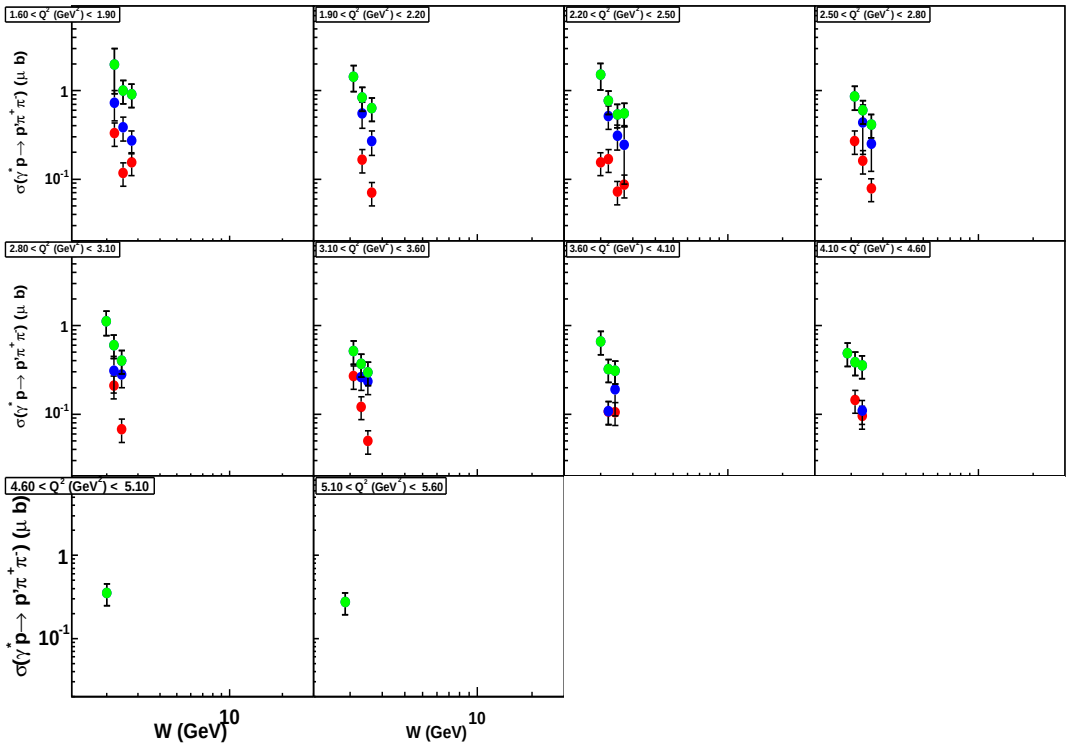

Figure 7: Reduced cross sections $\gamma^* p \to p\rho^0$ (green), $\gamma^* p \to p f_0$ (blue) and $\gamma^* p \to p f_2$ (red) as a function of W for constant Q^2 bins, in units of μbarn. The error bars include the quadrature addition of statistical and of the systematic uncertainties discussed in the text.

- 0-helicity state, the decay angular distribution should follow a $\cos(\theta_{HS})$ shape given by the $(Y_0^2)^2$ harmonics, i.e. $3\cos^2(\theta_{HS}) - 1$,
- 1-helicity state, the decay angular distribution should follow a $\cos(\theta_{HS})$ shape given by the $(Y_1^2)^2$ harmonics, i.e. $\sin^2(\theta_{HS})\cos^2(\theta_{HS})$,
- 2-helicity state, the decay angular distribution should follow a $\cos(\theta_{HS})$ shape given by the $(Y_2^2)^2$ harmonics, i.e. $\sin^4(\theta_{HS})$.

In Fig. 10, we see that the $\cos(\theta_{HS})$ distributions evolve with (x_B,Q^2) and that they probably involve a mixture of different helicity states. The analysis of these decay angular distributions imply a dedicated work and will be an important part of the final data analysis. This "disentanglement" of the various helicity contributions as a function of (x_B,Q^2) is interesting since, as we saw in the introduction, they correspond, at the leading-twist handbag approach, to different dominant mechanisms and various f_2 DA configurations.

Finally, we show in Figs. 11 and 12 the differential cross sections $\frac{d\sigma}{dt}$ as a function of t for all (x_B,Q^2) bins for the f_0 and the f_2 respectively. We see that

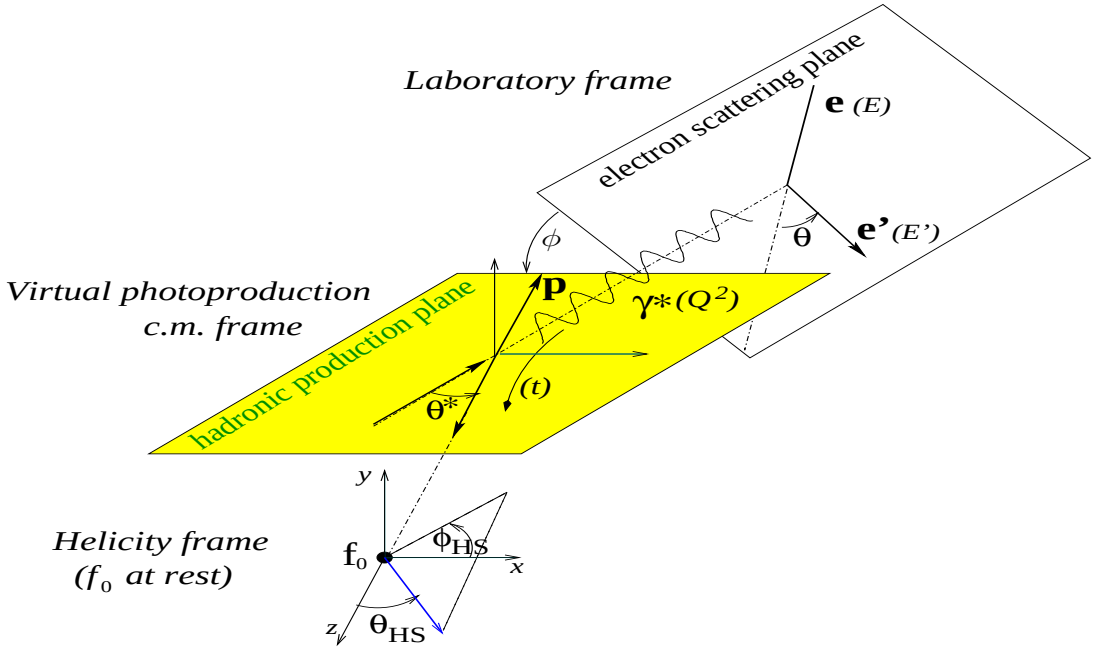

Figure 8: Reference frames and relevant variables for the description of the $ep \to e'pf_0 \hookrightarrow \pi^+\pi^-$ reaction. The system is the same for the ρ^0 and f_2 mesons.

$\frac{d\sigma}{dt}$ decreases with $-t$ increasing as could be expected, with, for both channels, some hints of a "drop" at low t (this latter feature is also observed in exclusive π^0 [12] and ρ^+ [11] production).

We fitted both distributions by a Ate^{bt} function, with A and b as free parameters. We display in Fig. 13 the fitted b parameter as a function of W for the ρ^0, f_0 and f_2 channels. We observe for the three channels the same behavior, i.e. that b increases with W. In a very crude approach, b can be interpreted as the size of the nucleon-meson system. The fact that it increases with W increasing, or equivalently increases with x_B decreasing (which is inversely proportional to W), can hint that the size of the nucleon increases as one probes smaller and smaller x_B, i.e. smaller and smaller parton momentum fractions.

3 Conclusion

We have presented in the first section a brief physics motivation for studying the exclusive channels $ep \to epf_0(980)$ and $ep \to epf_2(1270)$ (and more generally the whole process $ep \to ep\pi^+\pi^-$) above the resonance region. In the second section, we have shown, with a preliminary data analysis, that this study should be feasible with the CLAS e1-6 data.

In order to get publishable results, a certain number of steps and issues still need to be adressed. We mention a few of them:

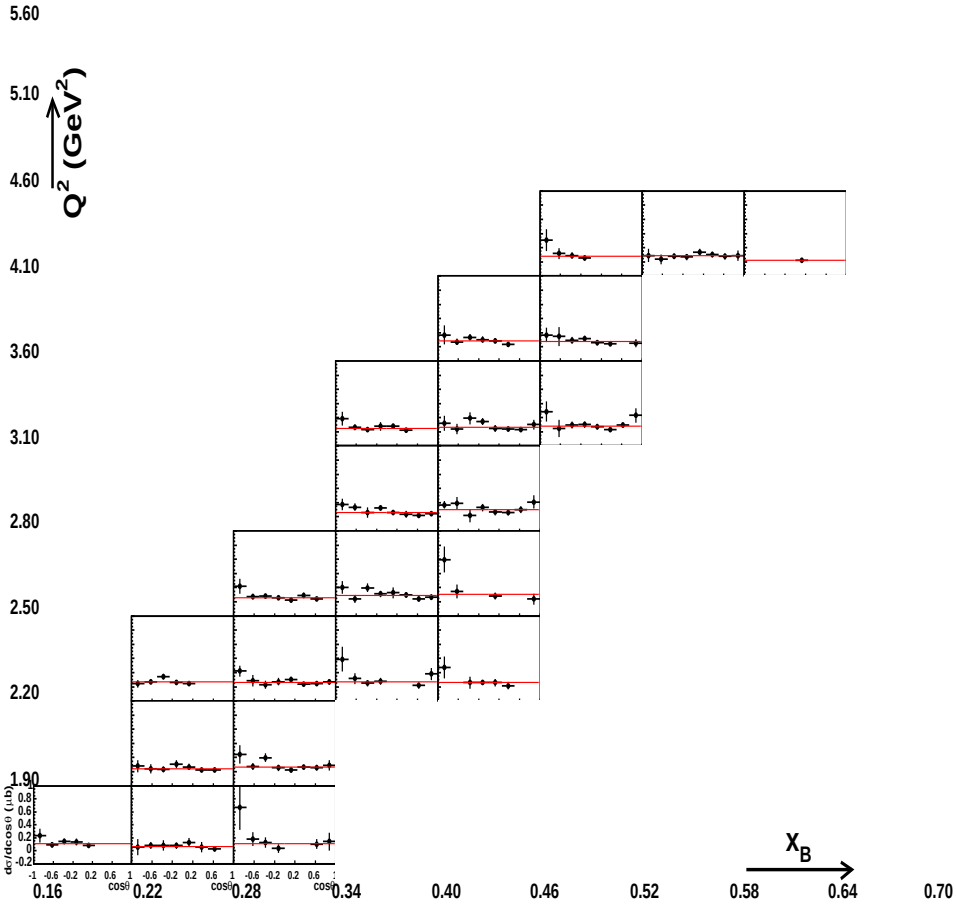

Figure 9: Cross section $d\sigma/d\cos(\theta_{HS})$ (in μb) for all bins in (Q^2,x_B) for the $ep \to epf_0(980)$ process. The red curve corresponds to the fit with a constant function.

- The experimental $\pi^+\pi^-$ invariant mass spectra of Fig. 5 need to be revisited and better understood. For instance, we see that the f_0 and f_2 peaks don't appear systematically centered at 980 MeV or 1270 MeV respectively. Are those "shifts" due to unprecise data analysis, such as uncorrect acceptance corrections, or rather to "true" physical interferences with the $\pi^+\pi^-$ continuum ? Also, there are sometimes some peaks which do not correspond to known mesonic states and which are therefore not expected to appear. For instance, in Fig. 5, in the ($0.22 < x_B < 0.28$, $1.90 < Q^2 < 2.20$) bin (upper right bin of the Fig. 5), there seems to be a peak between the f_0 and the f_2. Is it real or an artefact of an unprecise acceptance correction or some binning effect ? It was not crucial to understand these effects in order to extract the ρ^0 cross section since it is so broad and dominant (and that a $\approx 20\%$ systematic uncertainty was also introduced) but it is essential for the extraction of the f_0 and f_2 cross

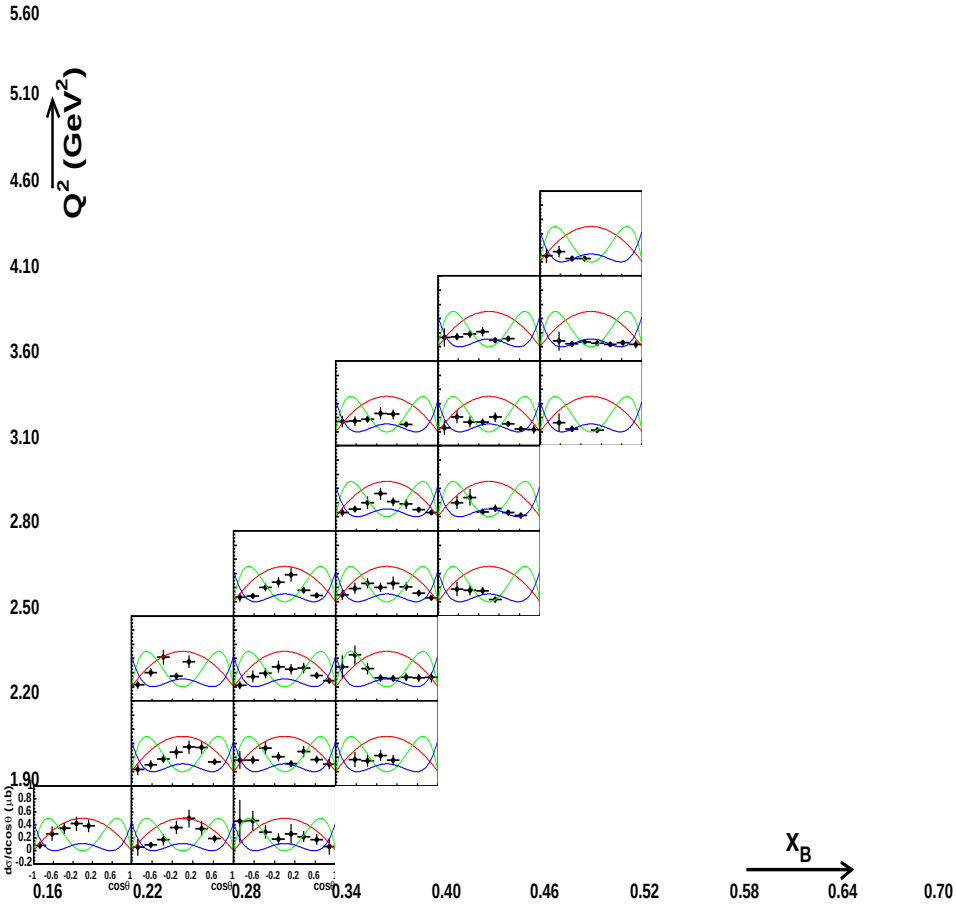

Figure 10: Cross section $d\sigma/d\cos(\theta_{HS})$ (in μb) for all bins in (Q^2,x_B) for the $ep \to epf_2(1270)$ process. The blue, red and green curves correspond to the $(Y_0^2)^2$, $(Y_1^2)^2$ and $(Y_2^2)^2$ harmonics respectively.

sections, which are quite weaker. We therefore plan to revisit in a very detailed manner the acceptance and binning of the e1-6 data, compared to what we did for the ρ^0 study.

- In parallel, as a corollary, this $\pi^+\pi^-$ invariant mass spectra also needs to be better understood *theoretically*. Many interfering channels contribute to the non-resonant $\pi^+\pi^-$ continuum. In order to extract small signals sitting over a large background, in particular such as the f_0, an understanding of the interference effects is needed. One should avoid to continue to do a background subtraction at the cross section level. All this can be adressed for instance by developping and extending the range of validity of the JM model [19], which describes rather succesfully the $ep \to ep\pi^+\pi^-$ reaction in the resonance region.

- As already mentioned, the analysis of the angular distributions of the

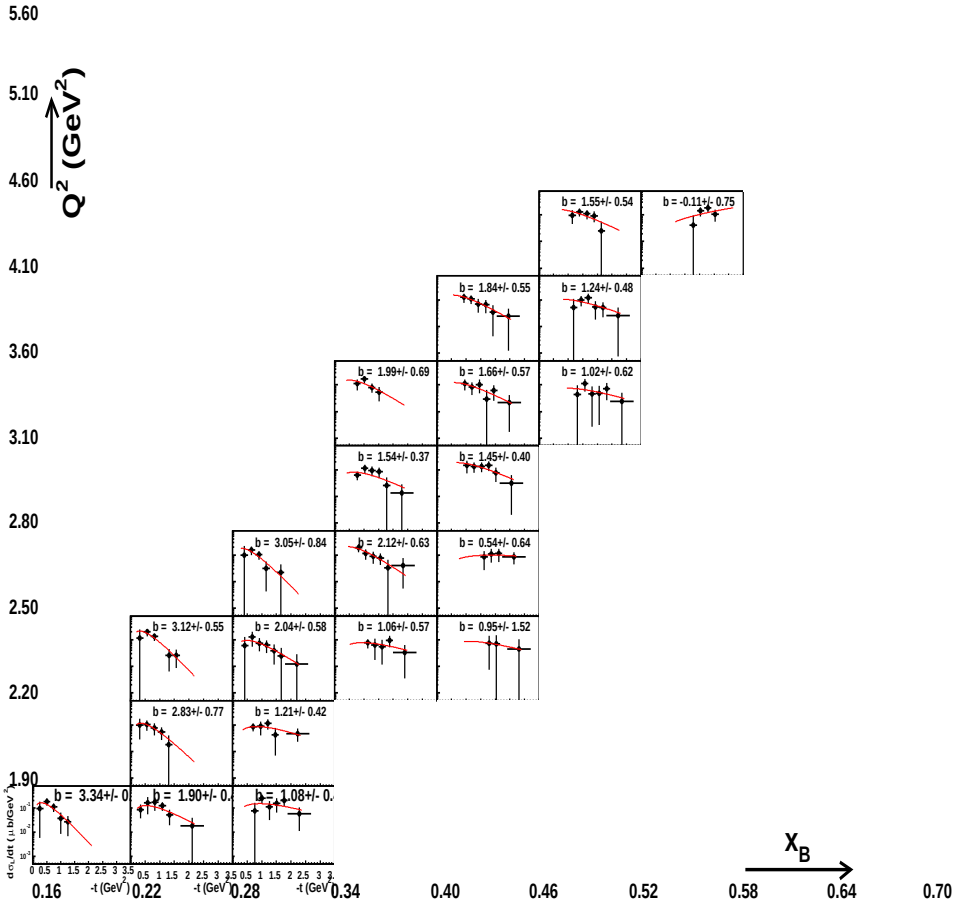

Figure 11: Cross section $d\sigma/dt$ (in μb/GeV^2) for all bins in (Q^2,x_B) as a function of $-t$ (in GeV^2) for the $ep \to epf_0(980)$ process. The red line shows the fit of the data by the function Ate^{bt}.

f_2 decay needs a dedicated effort in order to disentangle the various helicity components. More ambitiously, it would be interesting to extract the full set of Spin-Density Matrix Elements which means analyzing 3-dimensionnal angular distributions (i.e., the correlated ϕ_{HS} and ϕ angular dependences, in addition to the $\cos(\theta_{HS})$ one; see Fig. 8). This has actually not been done for the ρ^0 channel for which only 1-dimensionnal angular distributions were studied and this can also be part of the proposed analysis.

- Benefitting from the experience gained in the CLAS analysis of the exclusive *photoproduction* of the f_0 meson [20], we plan to try to carry out a partial wave analysis. This is a powerful technique in order to disentangle the resonant $\pi^+\pi^-$ contributions from the non-resonant ones.

We estimate that our group can carry out this analysis in roughly 1 to 2

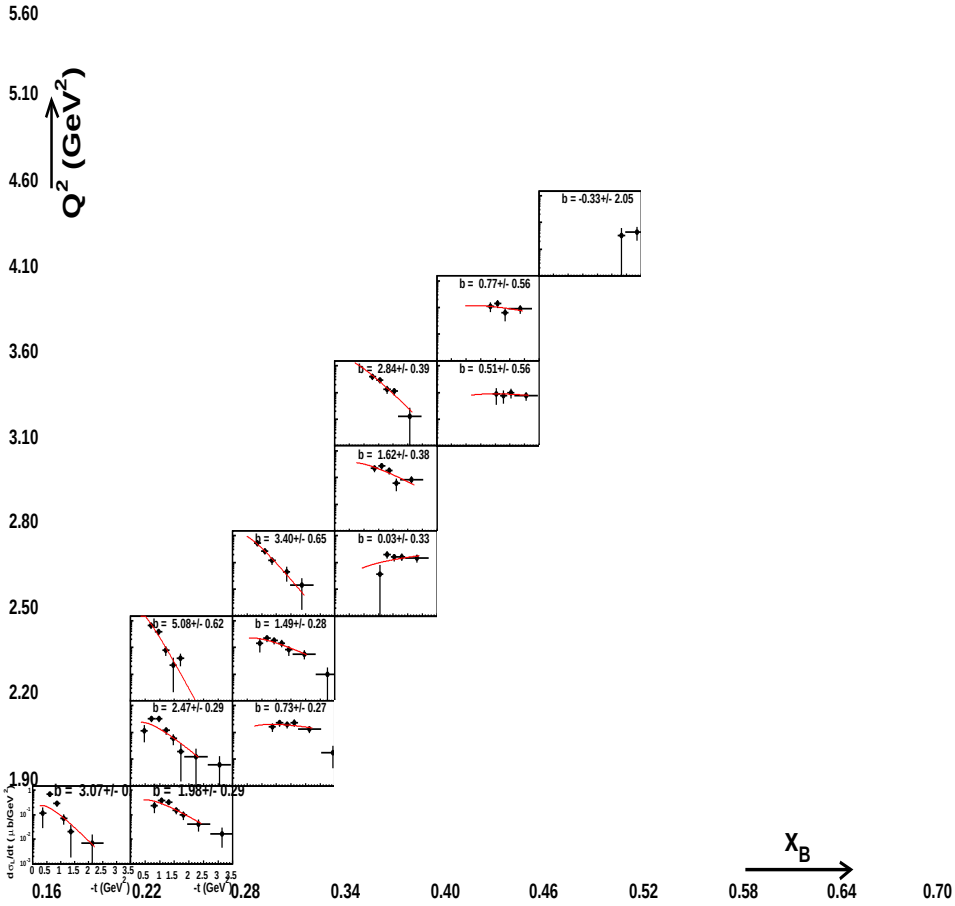

Figure 12: Cross section $d\sigma/dt$ (in μb/GeV^2) for all bins in (Q^2,x_B) as a function of $-t$ (in GeV^2) for the $ep \to epf_2(1270)$ process. The red line shows the fit of the data by the function Ate^{bt}.

years. We thus request a CAA from the DPWG/CLAS collaboration.

References

[1] K. Nakamura et al. (Particle Data Group), J. Phys. G 37, 075021 (2010).

[2] D. V. Bugg, Phys. Rept. 397, 257 (2004).

[3] A. Donnachie and Yu.S. Kalashnikova, arXiv:0806.3698 [hep-ph].

[4] L. S. Geng et al., AIP Conf. Proc. 1322, 214 (2010).

[5] J. C. Collins, L. Frankfurt, and M. Strikman, Phys. Rev. D 56, 2982 (1997).

[6] T. Horn et al., Phys. Rev. C 78, 058201 (2008).

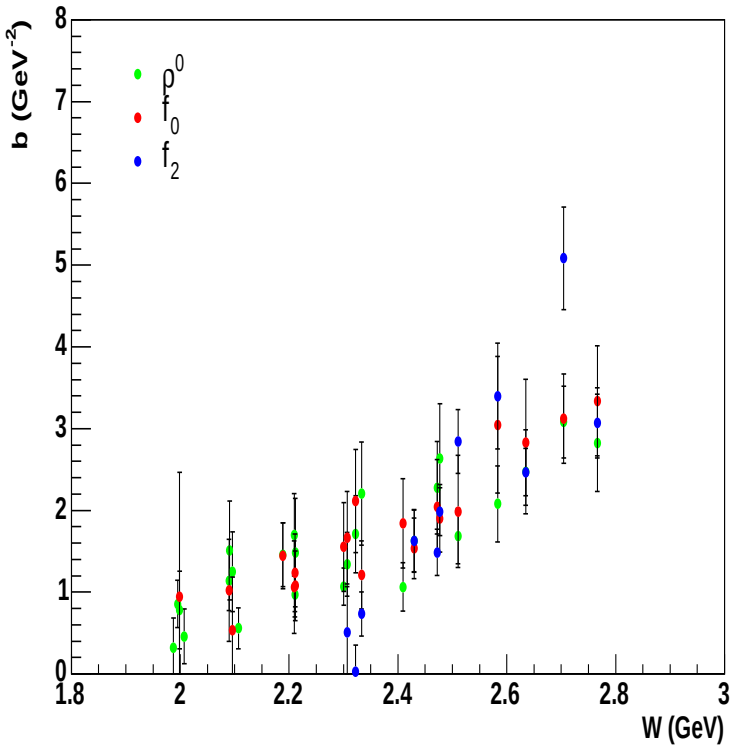

Figure 13: Slope b of $d\sigma/dt$ as a function of W. Green points: ρ^0, blue points: f_0, red points: f_2.

[7] E. Fuchey et al., Phys.Rev.C 83, 025201 (2011).

[8] S. A. Morrow et al., Eur. Phys. J. A 24, 5 (2009).

[9] L. Morand et al., Eur. Phys. J. A 24 445 (2005).

[10] J. P. Santoro et al., Phys. Rev. C 78, 025210 (2008).

[11] A. Fradi, PhD thesis, Orsay University (2010).

[12] I. Bedlinsky, PhD thesis, Moscow University (under progress).

[13] S.V. Goloskokov, P. Kroll, Eur. Phys. J. A 47, 112 (2011).

[14] V. Braun andN. Kivel,Phys. Lett. B 501, 48 (2001).

[15] B. Lehmann-Dronke, P. V. Pobylitsa, M. V. Polyakov, A. Schaefer and K. Goeke, Phys. Lett. B 475, 147 (2000).

[16] B. Lehmann-Dronke, A. Schaefer, M. V. Polyakov and K. Goeke, Phys. Rev. D 63, 114001 (2001).

[17] N. Warkentin,M. Diehl,D.Yu. Ivanov,A. Schaefer, Eur.Phys.J. A32, 273 (2007).

[18] M. Diehl, T. Gousset, B. Pire, Phys. Rev. D 62, 073014 (2000).

[19] V. I. Mokeev et al., Phys. Rev. C80, 045212 (2009).

[20] M. Battaglieri et al., Phys. Rev. Lett. 102, 102001 (2009).